Analyst

PAPER

View Article Online
View Journal





Cite this: DOI: 10.1039/d0an00249f

# Establishment of a universal and sensitive plasmonic biosensor platform based on the hybridization chain reaction (HCR) amplification induced by a triple-helix molecular switch†

Ganglin Wang, [a] Jingfeng Li, [b] Yong He,[c] Jun Liu,[d] Mingxia Yu[e] and Guoping Wang*[a]

Received 5th February 2020,
Accepted 20th March 2020

DOI: 10.1039/d0an00249f

rsc.li/analyst

Herein, we established a universal and sensitive plasmonic sensing strategy for biomolecule assays by coupling the hybridization chain reaction (HCR) strategy and a triple-helix molecular switch. Upon the recognition of the target, a single-stranded DNA as a universal trigger (UT) was released from the triple-helix molecular switch (THMS). Thus, the HCR process can be triggered between two hairpins M1 and M2, resulting in the aggregation of gold nanoparticles (AuNPs) *via* the hybridization between the tail sequence on M1 (or M2) and a DNA–AuNP probe with a dramatic change in the absorbance at 521 nm. More specifically, the strategy, which was conducted by the introduction of target-specific recognition of THMS and universalized by virtue of altering the aptamer or DNA sequence without changing the triple-helix structure, enables simple design for multiple target detection. By taking advantage of THMS, this strategy could enable stable and sensitive detection of a variety of targets including nucleic acids, small molecules and proteins, which may possess great potential for practical applications.

## Introduction

Changes in the levels of a variety of biomolecules (for instance, proteins and nucleic acids) frequently serve as a basis for the establishment of biomarkers associated with the onset and progression of many diseases, such as cancer.[1–3] Therefore, the construction of effective strategies and probes that allow the sensitive and reliable detection of biomarkers is vastly demanded for early disease diagnosis and further prognostic evaluation. Nevertheless, to the best of our knowledge, the concentration of these relevant biomarkers is usually low,[4] which makes their simple, sensitive, and cost-effective detection still challenging.

Over the past decades, a broad range of approaches such as western blotting,[5,6] enzyme-linked immunosorbent assay (ELISA),[7,8] mass spectrometry,[9,10] microarrays,[11,12] and electrochemical and photoelectrochemical methods[13–19] have been proposed for the highly sensitive detection of biomarkers. Meanwhile, some optical methods (fluorescent or colorimetric assays),[20–23] chemiluminescence method,[24] electrochemiluminescence (ECL) method,[25] Raman microspectroscopy and surface plasmon resonance (SPR)[26–28] have also been developed to detect a number of biomarkers. However, some of these techniques are usually time-consuming, may require expensive instrumentation and professional personnel and/or lack sufficient sensitivity, therefore restricting their applications towards rapid and sensitive biomarker detection. Due to the broad range of disease-related biomarkers, universal applicability is another essential requirement for the effective development of sensitive platforms. In this case, the detection of different analytes can be implemented by employing similar working principles and if possible limited modifications. Therefore, a convenient, universal and reliable method for detecting multiple biomarkers is still an urgent need and a challenging step for most platforms of biomarker identification.

Strategies involving nucleic acid-based signal amplification have currently gained comprehensive attention towards bio-

[a]Hubei Bioinformatics & Molecular Imaging Key Laboratory, Department of Biomedical Engineering, College of Life Science and Technology, Huazhong University of Science and Technology, Wuhan 430074, P. R. China. E-mail: wangguoping@hust.edu.cn
[b]Department of Orthopedics, Zhongnan Hospital of Wuhan University, Wuhan 430071, P. R. China
[c]Department of Nuclear Medicine and PET Center, Zhongnan Hospital of Wuhan University, Wuhan 430071, P. R. China
[d]School of Power and Mechanical Engineering, Wuhan University, Wuhan 430071, P. R. China
[e]Department of Clinical Laboratory, Zhongnan Hospital of Wuhan University, Wuhan 430071, P. R. China

†Electronic supplementary information (ESI) available: See DOI: 10.1039/d0an00249f

sensor applications, and these include rolling cycle amplification (RCA),[29] catalytic hairpin assembly (CHA),[30] strand displacement amplification (SDA),[31,32] hybridization chain reaction (HCR)[33,34] and cyclic enzymatic amplification (CEA).[35] Among these strategies, HCR involves a cascade of hybridization reactions triggered by initiators or target molecules in an enzyme-free environment at room temperature.[33] Due to its enzyme-free features, autonomous protocol and efficient isothermal amplification capability, HCR has been extensively utilized in the fields of bioanalysis and bioimaging. More recently, He and co-workers also reported a novel HCR-based strategy for virus detection.[36] In addition, Yang and colleagues developed an HCR-based ratiometric biosensor for the ultrasensitive detection of microRNA-133a.[37] In consideration of these putative advantages, the HCR amplification strategy appears to be the ideal platform for signal amplification in biomarker sensing and quantification.

In the past decades, nucleic acid triplex (NAT) structures have attracted considerable attention due to some advantages including simplified synthesis, convenient modification and high stability.[38] Traditionally, NAT is constructed by binding a third DNA strand to a double-helical DNA *via* Hoogsteen hydrogen bonds. As an important component of the DNA nanotechnology toolbox, NAT has evolved as a powerful tool for numerous applications in the fields of bioimaging,[39] drug delivery and biosensing.[40,41] The incorporation of a third DNA strand into the stem of molecular beacons to further form a triple-helix molecular switch (THMS) structure is an alternative strategy for the construction of biosensors. For instance, Li and coworkers have constructed a THMS-based bioanalytical platform for the highly sensitive and homogeneous electrochemical detection of melamine.[42] More recently, Liu and co-workers have also developed an electrochemical strategy coupled with THMS for the detection of tetracyclines.[43]

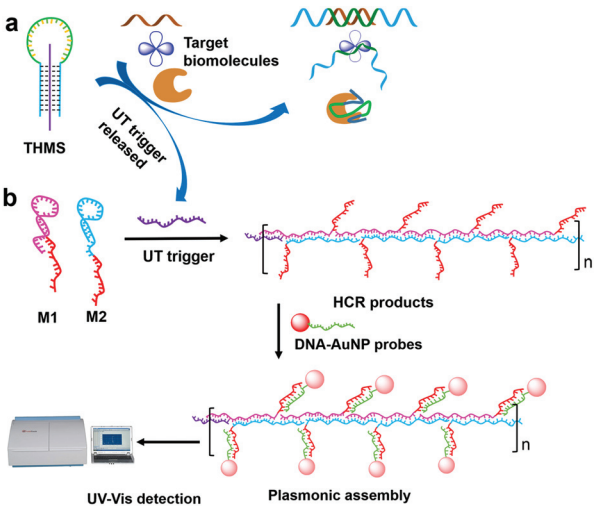


Fig. 1 Schematic of the design strategy for the plasmonic detection of targets based on the hybridization chain reaction amplification and the assembly of gold nanoparticles.

Considering the aforementioned aspects, here, we have presented a plasmonic strategy based on the aggregation of gold nanoparticles (AuNPs) coupled with THMS and HCR for the development of a sensitive assay for a broad range of targets. Thrombin (Tmb), adenosine triphosphate (ATP), and miRNA-21 were selected as the prototypical targets. As illustrated in Fig. 1, the unique structured THMS is prepared as follows: (i) a target-specific aptamer or DNA sequence served as the loop, (ii) two DNA segments flanked as the stems, and (iii) a DNA trigger matched simultaneously with the two respective stems. In the presence of a biomolecular target, the formed THMS was disassembled and then, the universal DNA trigger was released from THMS, activating the HCR process. The obtained HCR products could then hybridize with a DNA–AuNP probe, resulting in the aggregation of gold nanoparticles and a dramatic change in the absorbance at 521 nm. In this way, a highly sensitive and specific plasmonic approach was generated. More importantly, the universality of this strategy was achieved by basically altering the target-related sequence without changing the HCR system.

## Experimental

### Reagents and apparatuses

Hydrogen tetrachloroaurate trihydrate ($HAuCl_4 \cdot 3H_2O$, 99.9%) was purchased from Sigma-Aldrich. Tris(2-carboxyethyl) phosphine hydrochloride (TCEP, 98.0%) was acquired from TCI. Sodium citrate was purchased from J&K Scientific Ltd. Sodium hydroxide (NaOH, AR), hydrochloric acid (HCl, GR), acetic acid (HAc, AR), and nitric acid ($HNO_3$, GR) were purchased from Sinopharm Chemical Reagent Co., Ltd. Phosphate buffered saline (1× PBS) was purchased from Thermo Scientific (HyClone). Thrombin (Tmb), bovine serum albumin (BSA), immunoglobulin G (IgG), adenosine triphosphate (ATP), guanosine triphosphate (GTP), uridine triphosphate (UTP), cytidine triphosphate (CTP) and oligonucleotides were acquired from Sangon Biotech. Co., Ltd (Shanghai, China). All oligonucleotides were purified by HPLC. Water (18.2 MΩ) was purified by using a Milli-Q Direct-8 water purification system (Millipore). All other reagents and solvents that were utilized were of analytical grade. The sequences of the respective oligonucleotides used in this work are listed in Table S1.† Human blood samples were supplied by Wuhan Commercial Staff Hospital (CHN). All experiments were performed in accordance with the relevant laws and national guidelines (Ethical Guidelines for Biomedical Research on Human Participants, provided by China National Health and Family Planning commission) and approved by the Experimental Ethics Committee of Huazhong University of Science and Technology. Informed consents were obtained from the human participants of this study.

### Preparation of DNA–AuNP probes

Here, 13 nm AuNPs were synthesized using a previously reported method but with a minor modification.[44] Briefly,

30 mL of 0.01% (w/v) $HAuCl_4$ was boiled with vigorous stirring, and 0.9 mL trisodium citrate (1%, w/v) was further added into the boiling solution under agitation. The color of the solution turned from pale yellow to colorless and finally to burgundy. The reaction was performed for 15 minutes, and the resulting colloid was stirred until the solution reached room temperature. DNA–AuNP probes were prepared according to a salt-aging method.[44] Briefly, thiolated DNA was treated with TCEP (1 : 100 molar ratio) for 2 hours at room temperature in order to cleave the disulfide bond. Thiolated oligonucleotides were then added to a solution of GNPs (4 nM) at the final concentration of 1.2 μM under overnight agitation. After 12 h incubation, an SDS solution (10% w/v) was added to the mixture to achieve a final concentration of 0.1%. Phosphate buffer (0.1 M, pH 7.4) was further added to the mixture to achieve a final concentration of 0.01 M. In addition, the NaCl concentration of the mixture was slowly increased to 0.3 M over an eight-hour period. The final solution was centrifuged three times at 12 000 rpm for 10 min. After the supernatant was removed, DNA–AuNPs were resuspended in 400 μL of 1× PBS and stored at 4 °C.

### Construction of the triple-helix molecular switch (THMS) structure in an aqueous solution

Before adding the respective target molecules, triple-helix/UT structures were formed by adding a few microliters of extended aptamer to 0.5 mL of 100 nM UT. This addition was limited to 50 μL, resulting in a negligible change in volume. For Tmb and miRNA detection, the triple-helix aptamer or DNA sequence/UT structure complex was formed in PBS buffer having pH 6.2 and containing 100 mM NaCl, 20 mM KCl, and 2.5 mM $MgCl_2$ for 30 min at room temperature. For adenosine detection, the triple-helix aptamer/UT complex was formed in sodium phosphate buffer having pH 6.2 and containing 300 mM NaCl, 2.5 mM $MgCl_2$, and 0.1 mM EDTA for 30 min at 30 °C. Following the addition of the target molecules, the respective solutions were incubated for 30 min at room temperature.

### HCR and agarose gel electrophoresis

M1 and M2 probes were heated to 95 °C for 5 min and then allowed to cool to room temperature before use. A solution containing M1 (1.0 μM), M2 (1.0 μM), triple-helix aptamer/UT and aptamer/target complex was incubated at 37 °C for 2 h. Agarose gel electrophoresis was performed using 1× Tris-acetate (TA) buffer. Electrophoresis was performed at 120 V for 40 min in 1× TA buffer. Gel was further scanned using a gel image analysis system (GelDoc-310, UVP) under 365 nm UV excitiation.

### Procedure of the assay

HCR mixture (5 μL,1 μM) was added to 45 μL of 1× PBS buffer containing 4 nM DNA–AuNP probes. After thoroughly mixing and incubating this solution for ~8 h at room temperature (25 °C), the change in the AuNP solution was quantified according to the respective UV–Vis absorption spectra.

## Results and discussion

### Rationale for the development of a plasmonic target assay

The principle of the plasmonic sensing strategy, established here as a biomolecule-based platform, is based on coupling a hybridization chain reaction (HCR) with a triple-helix molecular switch (Fig. 1). This plasmonic sensing platform consists of two parts: the molecular recognition and signal transduction portions. The designed molecular recognition part is based on THMS, which consists of a central, target-specific aptamer (or a DNA sequence) flanked by two arm segments and a UT *via* Watson Crick (–) and Hoogsteen (·) base pairings. Meanwhile, the signal transduction part consists of hairpins M1 and M2 and DNA (*i.e.*, the AuNP probe). In the presence of the respective targets, the triple-helix aptamer/UT structure is perturbed due to the robust affinity of the target-specific aptamer or DNA sequence to its targets, liberating the UT trigger. Thereafter, the released UT trigger acts as an initiator to trigger the HCR process between M1 and M2 to form long nicked dsDNA. The obtained HCR products can then hybridize with the DNA–AuNP probe, resulting in the aggregation of gold nanoparticles with a dramatic change in the absorbance at 521 nm (monitored by spectroscopy). In accordance with this principle, signal transduction activity proportional to the target concentration can be finally determined.

### Feasibility of the plasmonic target assay

As a proof of concept, the HCR between UT and M1/M2 was first examined in a solution by agarose gel electrophoresis (Fig. 1). In the absence of UT, HCR was inhibited, whereas only a bright band of M1 and/or M2 could be observed (Fig. 2: lanes 2, 3, 5). By introducing UT, emission bands related to high-molecular-weight structures could be observed (Fig. 2: lanes 6–9), indicating the successful growth of long polymers in the presence of UT. Importantly, the longest product had over 500 base pairs, which might be highly efficient for signal amplification. It is worth noting that when we increase the concentration of the UT trigger, the length of the products becomes shorter (Fig. 2: lanes 5–9).

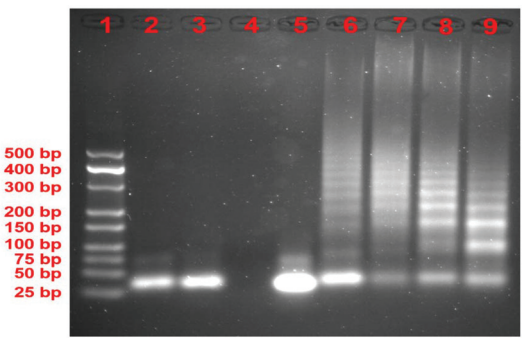


Fig. 2 3.5% agarose gel electrophoresis demonstrates UT-initiated HCR: lane 1: 25–500 bp ladder markers; lane 2, 1.0 μM M1; lane 3, 1.0 μM M2; lane 4, 1.0 μM UT; lanes 5–9, five different concentrations of UT (0.0, 0.1, 0.20, 0.50, and 1.0 μM) in a 1 μM mixture of M1 and M2.

For the additional validation of THMS complex formation and disassembly, we used gel electrophoresis to study the interaction of P1 and UT DNA strands. P1, UT and P1-UT THMS solutions were loaded on the agarose gel (3.5%) and visualized under UV light after staining with GelRed. As can be seen in Fig. S2,† the THMS complex appears as a single bright band, which is slightly slower than that of the P1 strand. These results indicated that the interaction between P1 and UT specifically occurred. It was also observed that in the presence of miRNA-21, a slower band occurred, indicating that the interaction between P1 and miRNA-21 was stronger, leading to the release of the UT strand. Thereafter, HCR was initiatied (Fig. S3†). Similar results can also be obtained for the P2-UT THMS-ATP (Fig. S4 and S5†) and P3-UT-Tmb (Fig. S6 and S7†) detection systems.

To demonstrate the feasibility of this strategy, confirmatory experiments were carried out for UT DNA detection. As shown in Fig. 3 B, in the absence of UT DNA, a surface plasmon resonance absorption peak at 521 nm is observed for the DNA–AuNP dispersion, suggesting the lack of assembly of gold nanoparticles in the absence of UT DNA. On the other hand, this absorbance band decreased significantly in the presence of 5.0 nM UT DNA. Alternatively, the UT DNA-induced aggregation of functionalized AuNPs was confirmed by dynamic light scattering (DLS) and transmission electron microscopy (TEM). The average hydrodynamic diameter of the dispersed DNA–AuNPs was around 22.3 nm (Fig. S1†). This diameter increased to 34.8 nm upon addition to the M1/M2 mixture (Fig. 3E). The morphology of the particles was characterized by TEM (Fig. 3C), indicating that DNA–AuNPs were well dispersed with a narrow size in the range of 13–17 nm. Upon the addition of 5.0 nM target DNA, the average hydrodynamic diameter of the functionalized AuNPs increased to 425.3 nm (Fig. 3F). Accordingly, these large DNA-linked three-dimensional aggregates were clearly observed by TEM (Fig. 3D).

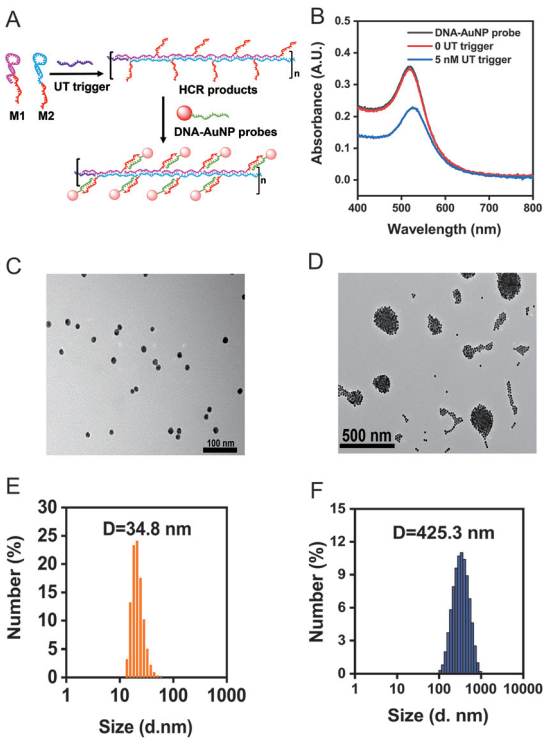


Fig. 3 (A) Schematic of UT-initiated plasmonic assembly. (B) UV-vis absorption spectra of the plasmonic sensing system in the absence and presence of target DNA (5.0 nM). (C) TEM image of the dispersed DNA–AuNPs. (D) TEM image of a microscopic DNA-functionalized AuNP assembly. (E) DLS measured hydrodynamic size distribution of the dispersed DNA-functionalized AuNPs. (F) DLS measured in the presence of 5.0 nM UT.

## Optimization of the sensing strategy

To achieve good performance for target assays, some experimental conditions should be optimized. As shown in Fig. S8A,† no obvious differences are observed in the temperature range of 25–37 °C, indicating that temperature has negligible influence on HCR. Therefore, 25–37 °C was selected in further experiments for the HCR reaction. Fig. S8B† shows the relationship between the product length and efficiency and HCR time; the maximum signal was achieved when the HCR time was longer than 2 h. Thus, an HCR reaction time of 2 h was selected for the subsequent experiments. We also investigated the effects of the aggregation time and temperature of DNA–AuNPs and HCR products. As shown in Fig. S8C and S8D,† the $\Delta A$ of the sensing system slightly changes. The best signal-to-noise ratio was obtained at an aggregation time of 8 h and temperature of 25 °C. Therefore, the optimal aggregation time and temperature were considered as 8 h and 25 °C, respectively.

## Detection of microRNA

To demonstrate the applicability of the proposed approach for the sensitive detection of nucleic acids, miRNA-21 was chosen as a prototypical target (sequences listed in Table S1†). As shown in Fig. 4A, the absorbance at 521 nm gradually decreases on increasing the miRNA concentration. It was also found that $\Delta A$ ($\Delta A$ = difference in the absorbance values of the peaks without target and with target) increased linearly with the concentration of miRNA-21 (in the range of 20–200 pM) with a limit of detection (LOD) of ~20 pM, which was calculated as three times the standard deviation of the signal corresponding to that of a blank sample[45,46] (Fig. 4B and C); this was comparable to previously reported results (Table S2†). The specificity of the sensing system was further investigated by adding several miRNA family members. As shown in Fig. 4D, a high $\Delta A$ value is obtained only in the presence of miRNA-21. The $\Delta A$ values of other miRNAs were comparable to the background signal. Altogether, these results demonstrate the high specificity of this proposed assay.

## Detection of ATP

After the validation of the plasmonic sensing strategy as a platform for nucleic acids analysis, we attempted to use this same approach to detect small molecules using adenosine triphosphate (ATP) as a model system. ATP, an important substrate

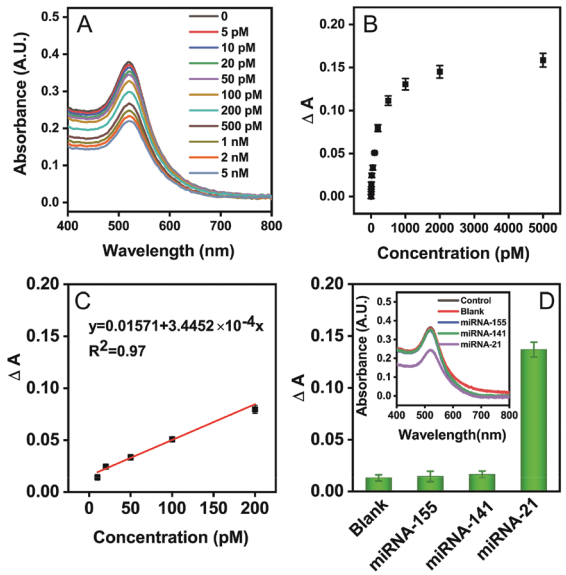


**Fig. 4** (A) UV-vis absorbance spectra of the sensing system in the presence of various concentrations of miRNA-21. (B) Plots of changes in absorbance (Δ*A*) *versus* the concentration of miRNA-21. (C) Calibration curve for concentrations ranging from 20 to 200 pM. (D) Changes in the absorbance (Δ*A*) of the sensing system in the presence of 1 nM miRNA-21 and other miRNAs.

in living cells, plays an important part in the regulation of metabolism by supplying energy for cellular activities. Therefore, the sensitive detection of ATP in an aqueous solution is of great significance. Our results based on this strategy indicated that the absorbance at 521 nm gradually decreased with an increase in ATP concentrations (Fig. 5A). As shown in Fig. 5C, a linear relationship is obtained between absorbance and concentration in a dynamic range of 20–500 nM. The LOD of this method for ATP was estimated to be 15.6 nM, which compared well with those of previously reported systems (Table S3†). In order to assess the specificity of the sensing system for ATP, respective analogs (*i.e.*, GTP, CTP, and UTP) were added into the reaction system. These analogs did not interfere with ATP detection (Fig. 5D), suggesting that the proposed strategy exhibited good performance for discriminating ATP against potential analogs.

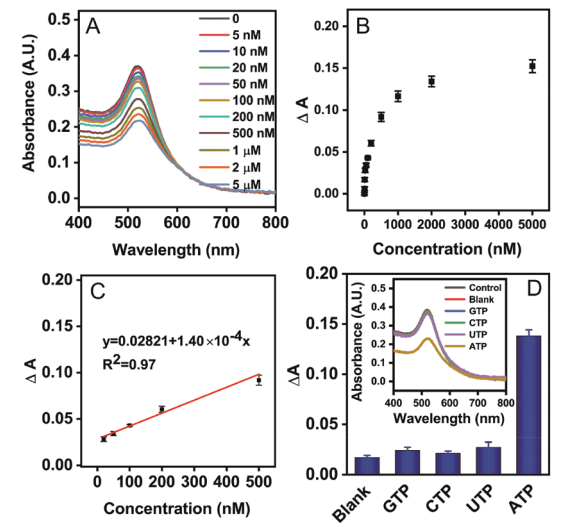


**Fig. 5** (A) UV-vis absorbance spectra of the sensing system in the presence of various ATP concentrations. (B) Plots of changes in absorbance (Δ*A*) *versus* ATP concentration. (C) Calibration curve for ATP concentrations ranging from 20 to 500 nM. (D) Changes in the absorbance (Δ*A*) of the sensing system in the presence of 1 μM ATP and respective analogs.

## Thrombin detection

To assess some universal applications, we further investigated whether the plasmonic sensing strategy could precisely detect proteins. For this, we tested a thrombin aptamer sequence flanked by two arm segments (Table S1; ESI†) to detect thrombin, an important factor involved in the coagulation cascade and platelet activations, which is also closely related to tumor cell transformation as well as tumor growth and progression. Therefore, experimental approaches that allow a highly sensitive and selective detection of thrombin are warranted. As shown in Fig. 6A, on increasing the addition of thrombin, the absorbance at 521 nm gradually decreases. The relationship between Δ*A* and the concentration of thrombin was also defined (Fig. 6C). A good linear correlation was obtained in the concentration range of 20–800 pM. The LOD of this method for thrombin was estimated to be 18.4 pM. The detection performance of the strategy was also comparable to that of some

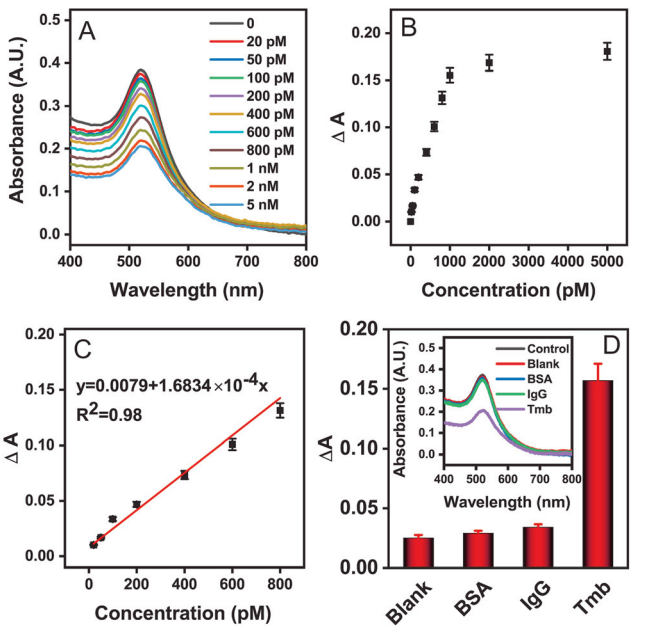


**Fig. 6** (A) UV-vis absorbance spectra of the sensing system in the presence of various thrombin concentrations. (B) Plots of changes in absorbance (Δ*A*) *versus* concentration. (C) Calibration curve for the concentrations of thrombin ranging from 20 to 800 pM. (D) Changes in the absorbance (Δ*A*) of the sensing system in the presence of 1 nM thrombin, BSA and IgG (controls).

Table 1 Recovery detection of miRNA-21 in 2% human serum (v/v) samples ($n$ = 3)

| Sample | Added | Found | Recovery (%) | RSD (%) |
|---|---|---|---|---|
| 1 | 30 pM | 33.2 pM | 110.7 | 4.7 |
| 2 | 100 pM | 104.3 pM | 104.0 | 7.9 |
| 3 | 200 pM | 196 pM | 98.0 | 6.2 |

Table 2 Recovery detection of ATP in 2% human serum (v/v) samples ($n$ = 3)

| Sample | Added | Found | Recovery (%) | RSD (%) |
|---|---|---|---|---|
| 4 | 30 nM | 28 nM | 93.3 | 3.1 |
| 5 | 100 nM | 103.1 nM | 103.1 | 4.6 |
| 6 | 300 nM | 321 nM | 107 | 5.7 |

Table 3 Recovery detection of thrombin in 2% human serum (v/v) samples ($n$ = 3)

| Sample | added | Found | Recovery (%) | RSD (%) |
|---|---|---|---|---|
| 7 | 30 pM | 32 pM | 106.7 | 5.3 |
| 8 | 100 pM | 104 pM | 104.0 | 4.7 |
| 9 | 300 pM | 295.8 pM | 98.6 | 6.4 |

reported methods (Table S4†). To investigate the specificity of the proposed strategy for thrombin, we selected two different proteins as controls: BSA and IgG. As shown in Fig. 6D, the $\Delta A$ value has no noticeable changes in the presence of IgG or BSA (1.0 nM), while the $\Delta A$ value greatly increases after the addition of thrombin (1.0 nM), demonstrating that the sensing system has a highly selective response to thrombin.

### Real sample assay

To evaluate other potential applications of the plasmonic sensing strategy, the detection of specific targets in fetal bovine serum (FBS) was also evaluated. Different target concentrations were added into diluted human serum (2% serum matrix). Each sample was analyzed three times (the experimental results are listed in Tables 1–3). The recovery results indicated good accuracy and reliability of the developed strategy when used in a real complex matrix. Based on the abovementioned results, we believe that this approach has promising applications in various chemical and biological laboratories for molecule-based assays in both pure solutions and complicated matrices mostly because it is easier to operate and cost-effective and has high sensitivity. Moreover, additional features such as universal applicability, enzyme-free and high selectivity are major contributors for the feasibility of this strategy.

## Conclusions

Here, we have successfully introduced a single plasmonic platform to detect multiple target analytes. The strategy design was based on the THMS-induced hybridization chain reaction amplification. The present approach can be engineered in ways that offer unique advantages and capabilities not available for conventional plasmonic detection systems. In the presence of different analytes, the modification of the label-free aptamer (or DNA sequences) in the triple helix structure can be achievable. As such, this strategy is well versatile due to the ability to select different types of aptamers for probe capture. Given the low cost, ultra-high sensitivity, and excellent generality, we anticipate that the single plasmonic strategy might evolve into a universal platform for a broad range of targets to be utilized in high-throughput drug screening.

## Conflicts of interest

There are no conflicts to declare.

## Acknowledgements

The authors gratefully acknowledge financial support of the National Natural Science Foundation of China (61875062, 81871752, 81871391, 51305307, 81472033, 30901308), the Fundamental Research Funds for the Central Universities and Hubei Province health and family planning scientific research project (WJ2015Q021).

## Notes and references

1 C. L. Sawyers, *Nature*, 2008, **452**, 548–552.
2 L. Wu and X. Qu, *Chem. Soc. Rev.*, 2015, **44**, 2963–2997.
3 C. A. Borrebaeck, *Nat. Rev. Cancer*, 2017, **17**, 199–204.
4 M. Zellner, R. Babeluk, M. Diestinger, P. Pirchegger, S. Skeledzic and R. Oehler, *Electroanalysis*, 2008, **29**, 3621–3627.
5 X. X. Han, H. Y. Jia, Y. F. Wang, Z. C. Lu, C. X. Wang, W. Q. Xu, B. Zhao and Y. Ozaki, *Anal. Chem.*, 2008, **80**, 2799–2804.
6 J. Liang, H. Liu, C. Huang, C. Yao, Q. Fu, X. Li, D. Cao, Z. Luo and Y. Tang, *Anal. Chem.*, 2015, **87**, 5790–5796.
7 C. Li, Y. Yang, D. Wu, T. Li, Y. Yin and G. Li, *Chem. Sci.*, 2016, **7**, 3011–3016.
8 E. P. Diamandis, *Mol. Cell. Proteomics*, 2004, **3**, 367–378.
9 C. A. Crutchfield, S. N. Thomas, L. J. Sokoll and D. W. Chan, *Clin. Proteomics*, 2016, **13**, 1.
10 H. Lu, H. Zhang, Y. Wei and H. Chen, *Analyst*, 2020, **145**, 313–320.
11 A. Belushkin, F. Yesilkoy and H. Altug, *ACS Nano*, 2018, **12**, 4453–4461.
12 D. Brambilla, M. Chiari, A. Gori and M. Cretich, *Analyst*, 2019, **144**, 5353–5367.
13 M. Hasanzadeh, N. Shadjou and M. de la Guardia, *TrAC, Trends Anal. Chem.*, 2017, **91**, 67–76.
14 S. Liu, Z. Yang, Y. Chang, Y. Chai and R. Yuan, *Biosens. Bioelectron.*, 2018, **119**, 170–175.

 

15 J. Yang, Y. Wu, C. Gan, R. Yuan and Y. Xiang, *Biosens. Bioelectron.*, 2018, **117**, 743–747.
16 J. Chang, X. Wang, J. Wang, H. Li and F. Li, *Anal. Chem.*, 2019, **91**, 3604–3610.
17 P. Gai, C. Gu, H. Li, X. Sun and F. Li, *Anal. Chem.*, 2017, **89**, 12293–12298.
18 T. Hou, N. Xu, W. Wang, L. Ge and F. Li, *Anal. Chem.*, 2018, **90**, 9591–9597.
19 Y. Wang, L. Xia, C. Wei, H. Wang, H. Wang, R. Yuan and S. Wei, *Chem. Commun.*, 2019, **55**, 13082–13084.
20 D. Wu, A. C. Sedgwick, T. Gunnlaugsson, E. U. Akkaya, J. Yoon and T. D. James, *Chem. Soc. Rev.*, 2017, **46**, 7105–7123.
21 Y. Li, D. Jia, W. Ren, F. Shi and C. Liu, *Adv. Funct. Mater.*, 2019, **29**, 1903191.
22 H. Ye, K. Yang, J. Tao, Y. Liu, Q. Zhang, S. Habibi, Z. Nie and X. Xia, *ACS Nano*, 2017, **11**, 2052–2059.
23 J. Hahn, E. Kim, Y. You and Y. J. Choi, *Analyst*, 2019, **144**, 4439–4446.
24 X. Jie, H. Yang, M. Wang, Y. Zhang, W. Wei and Z. Xia, *Angew. Chem., Int. Ed.*, 2017, **56**, 14596–14601.
25 H. Qi and C. Zhang, *Anal. Chem.*, 2020, **92**, 524–534.
26 K. K. Reza, J. Wang, R. Vaidyanathan, S. Dey, Y. Wang and M. Trau, *Small*, 2017, **13**, 1602902.
27 Y. Li, H. J. Lee and R. M. Corn, *Anal. Chem.*, 2007, **79**, 1082–1088.
28 U. Eletxigerra, J. Martinez-Perdiguero, R. Barderas, J. M. Pingarrón, S. Campuzano and S. Merino, *Anal. Chim. Acta*, 2016, **905**, 156–162.
29 Q. Yao, Y. Wang, J. Wang, S. Chen, H. Liu, Z. Jiang, X. Zhang, S. Liu, Q. Yuan and X. Zhou, *ACS Nano*, 2018, **12**, 6777–6783.
30 J. Liu, Y. Zhang, H. Xie, L. Zhao, L. Zheng and H. Ye, *Small*, 2019, **15**, 1902989.
31 Y. Li, S. Liu, Z. Zhao, Y. Zheng and Z. Wang, *Talanta*, 2017, **164**, 196–200.
32 F. C. Simmel, B. Yurke and H. R. Singh, *Chem. Rev.*, 2019, **119**, 6326–6369.
33 R. M. Dirks and N. A. Pierce, *Proc. Natl. Acad. Sci. U. S. A.*, 2004, **101**, 15275.
34 S. Bi, S. Yue and S. Zhang, *Chem. Soc. Rev.*, 2017, **46**, 4281–4298.
35 H. Dong, H. Chen, J. Jiang, H. Zhang, C. Cai and Q. Shen, *Anal. Chem.*, 2018, **90**, 4507–4513.
36 M. Du, G. Mao, S. Tian, Y. Liu, J. Zheng, X. Ke, Z. Zheng, H. Wang, X. Ji and Z. He, *Anal. Chem.*, 2019, **91**, 15099–15106.
37 L. Zhu, J. Ye, S. Wang, M. Yan, Q. Zhu, J. Huang and X. Yang, *Chem. Commun.*, 2019, **55**, 11551–11554.
38 G. Felsenfeld, D. R. Davies and A. Rich, *J. Am. Chem. Soc.*, 1957, **79**, 2023–2024.
39 Y. Yamagata, T. Emura, K. Hidaka, H. Sugiyama and M. Endo, *Chem. – Eur. J.*, 2016, **22**, 5494–5498.
40 X. Chen, T. Chen, L. Ren, G. Chen, X. Gao, G. Li and X. Zhu, *ACS Nano*, 2019, **13**, 7333–7344.
41 J. Zheng, J. Li, Y. Jiang, J. Jin, K. Wang, R. Yang and W. Tan, *Anal. Chem.*, 2011, **83**, 6586–6592.
42 X. Liu, M. Song and F. Li, *Sci. Rep.*, 2017, **7**, 4490.
43 Y. Wang, L. Yao, G. Ning, Y. Wu, S. Wu, S. Mao and G. Q. Liu, *Biosens. Bioelectron.*, 2019, **143**, 111613.
44 N. Li, C. Chang, W. Pan and B. Tang, *Angew. Chem., Int. Ed.*, 2012, **51**, 7426–7430.
45 M. Li, J. Zhang, S. Suri, L. J. Sooter, D. Ma and N. Wu, *Anal. Chem.*, 2012, **84**, 2837–2842.
46 Y. Wei, Y. Chen, H. Li, S. Shuang, C. Dong and G. Wang, *Biosens. Bioelectron.*, 2015, **63**, 311–316.